



1

2

3

4

5

6 Iron isotopes reveal significant aerosol dissolution over the Pacific Ocean

7

8

9

10 Authors: Capucine Camin¹, François Lacan¹, Catherine Pradoux¹, Marie Labatut¹, Anne
11 Johansen², James W. Murray³

12 ¹ UNIVERSITE DE TOULOUSE, LEGOS (CNES/CNRS/IRD/UT3), TOULOUSE, FRANCE

13 ²CENTRAL WASHINGTON UNIVERSITY, ELLENSBURG, WASHINGTON, USA

14 ³SCHOOL OF OCEANOGRAPHY, UNIVERSITY OF WASHINGTON, SEATTLE, WASHINGTON, USA

15

16 Corresponding authors: Camin C. and Lacan F., LEGOS, 14 Avenue Edouard Belin, F-31400
17 Toulouse, France (capucine.camin@orange.fr and francois.lacan@cnrs.fr).

18

19



20 **Abstract**

21

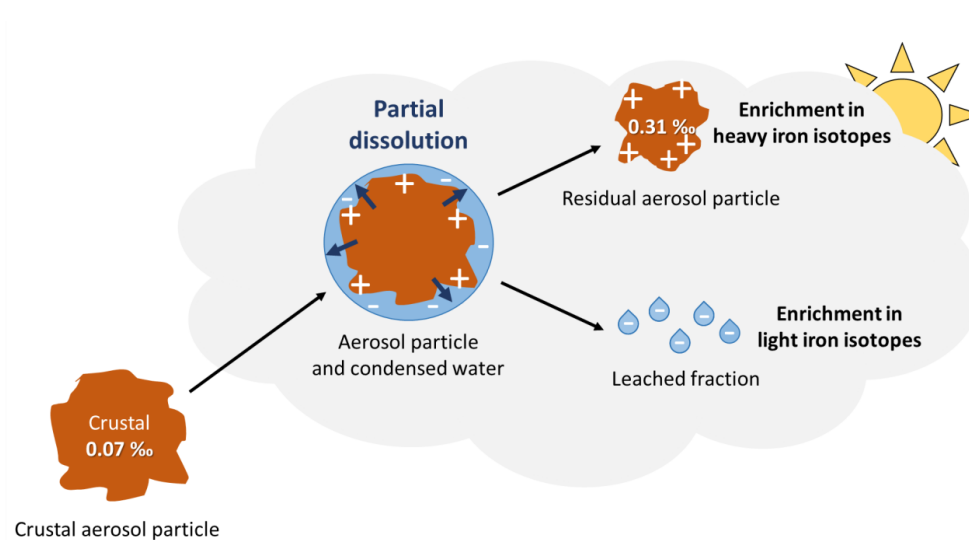
22 This study presents aerosol iron isotopic compositions ($\delta^{56}\text{Fe}$) in Western and Central
23 Equatorial and Tropical Pacific Ocean. Aerosols supply iron (Fe), a critical element for marine
24 primary production, to the open ocean. Particulate aerosols, $> 1 \mu\text{m}$, were sampled during
25 EUCFe cruise (RV *Kilo Moana*, PI: J. W. Murray, 2006). One aerosol sample was isotopically
26 lighter than the crust ($\delta^{56}\text{Fe} = -0.16 \pm 0.07 \text{‰}$, 95 % confidence interval), possibly originating
27 from combustion processes. The nine other aerosol samples were isotopically heavier than the
28 crust, with a rather homogeneous signature of $0.31 \pm 0.21 \text{‰}$ (2SD, $n=9$). Given i) this
29 homogeneity compared to the diversity of their modeled geographic origin and ii) the values of
30 the Fe/Ti ratios used as a lithogenic tracer, we suggest that these heavy $\delta^{56}\text{Fe}$ signatures reflect
31 isotopic fractionation of crustal aerosols caused by atmospheric processes. Using a fractionation
32 factor of $\Delta_{\text{solution - particle}} = -1.1 \text{‰}$, a partial dissolution of $\approx 20 \%$ of the initial aerosol iron content,
33 followed by the removal of this dissolved fraction, would explain the observed slightly heavy
34 Fe isotope signatures. Such fractionation has been observed previously in laboratory
35 experiments, but never before in a natural environment. The removal of the dissolved fraction
36 of the aerosols has not been previously documented either. This work illustrates the strong
37 constrains provided by the use of iron isotopes for atmospheric process studies.

38

39 Key words: Iron Isotopes, Aerosols, Equatorial and Tropical Pacific, Partial Dissolution,
40 Fractionation

41

42 **Graphical Abstract**



43

44

45 Key points

- 46 • Iron isotope fractionation of particle aerosol during atmospheric transport
- 47 • Preferential dissolution and subsequent removal of the dissolved fraction

48

49

50



51 1. INTRODUCTION

52 Iron (Fe) is an essential micronutrient for phytoplankton, playing a key role in primary
53 production, nitrogen fixation and community structures (Boyd and Ellwood, 2010; Morel et al.,
54 2020). Availability and speciation of this micronutrient impact the global carbon cycle and
55 climate. In some areas of the open ocean, low concentrations of Fe can limit primary production
56 (Martin, 1992). Five predominant sources of bioavailable Fe to the global ocean are currently
57 thought to be aerosol dissolution (Duce and Tindale, 1991; Jickells et al., 2005; Moore and
58 Braucher, 2008), sediment dissolution and resuspension (Elrod et al., 2004; Radic et al., 2011;
59 Labatut et al., 2014), fluvial inputs (Poulton and Raiswell, 2002), hydrothermal vents
60 (Tagliabue et al., 2010; Resing et al., 2015) and locally ice melting (Raiswell et al., 2008). Iron
61 sources to the open ocean remain insufficiently understood.

62 For about twenty years, it has become possible to measure iron isotopes in the
63 environment. The isotopic composition is expressed by $\delta^{56}\text{Fe}$ in ‰ which shows the deviation
64 of the sample's $^{56}\text{Fe}/^{54}\text{Fe}$ ratio relative to the reference material IRMM-14 (Eq. 1):

$$65 \delta^{56}\text{Fe} = \frac{(^{56}\text{Fe}/^{54}\text{Fe})_{\text{sample}}}{(^{56}\text{Fe}/^{54}\text{Fe})_{\text{IRMM-14}}} - 1 \quad (1)$$

66 With this definition, the upper continental crust is characterized by an homogeneous signature
67 of $\delta^{56}\text{Fe} = 0.07$ ‰ (Poitrasson, 2006). Iron isotopes measurements have led to significant
68 advances in our understanding of the cycle of this element (Radic et al., 2011; John et al., 2012;
69 Conway and John, 2014; Abadie et al., 2017; Klar et al., 2018). However, isotopic studies on
70 aerosols in marine environments are still very rare.

71 Aerosols have been found to span a large range of $\delta^{56}\text{Fe}$ values, from -3.91 ‰ (Kurisu
72 et al., 2016b) to 0.80 ‰ (Flament et al., 2008). Natural and anthropogenic sources are
73 associated with specific ranges of Fe isotope signatures (Wang et al., 2022). Natural sources of
74 aerosols are rocks, soils, loess, seawater, river water, volcanoes, plants and biomass burning.
75 Anthropogenic ones are mainly derived from combustion processes such as coal burning,



76 metallurgy, waste incineration and vehicle exhaust (Kommalapati and Valsaraj, 2009).
77 Therefore, iron isotopes can be used to identify aerosol sources. Nevertheless, initial aerosol
78 isotope signatures may be modified through isotope fractionations during atmospheric
79 transport. Such fractionation can complicate interpretation of isotopic signatures as source
80 tracers. Laboratory experiments have documented Fe isotope fractionation due to aerosol partial
81 dissolution (Mulholland et al., 2021; Maters et al., 2022). However, such fractionation has not
82 been evidenced from in situ data. This is only one potential explanation among others to
83 understand iron isotope signature of aerosols during field study (Kurusu et al., 2021). Aerosol
84 Fe isotopic data are scarce in oceanic environments, and none have been reported in the
85 Equatorial Pacific, despite the important role of iron as a limiting micronutrient in the Eastern
86 Equatorial Pacific.

87 This article presents iron isotope data from these aerosols collected in the Equatorial and
88 Tropical Pacific. Combined with elemental concentration data and modeled back trajectories,
89 these isotopic data provide new constraints on the processes involved in the aerosol iron cycle
90 during their transport.

91

92 **2. SAMPLING LOCATIONS AND METHODS**

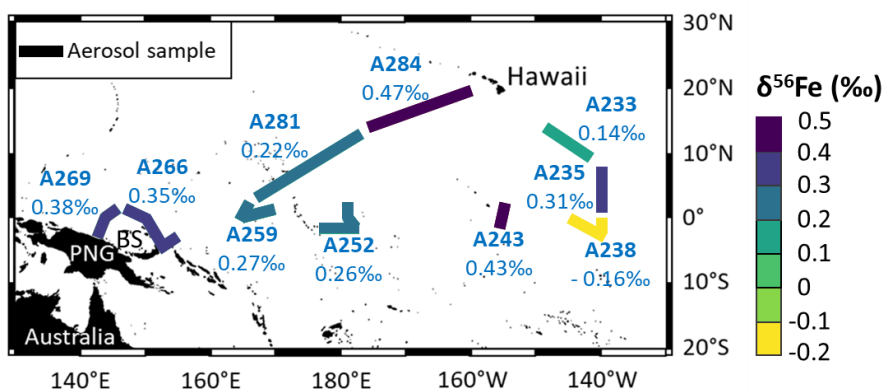
93 **2.1. AEROSOL SAMPLING**

94 Atmospheric particles were sampled during the EUcFe cruise (August – October 2006,
95 R/V *Kilo Moana*, Chief Scientist J. W. Murray). This cruise was carried out to study the iron
96 cycle, including atmospheric deposition, in the Equatorial and Tropical Pacific. Samples were
97 collected along the cruise track with a small volume collector equipped with 1 µm porosity
98 47 mm diameter PTFE membranes, placed in a Millipore® polycarbonate filter holder. The
99 membranes had previously been acid cleaned with in HNO₃ for 2 days and stored in clean
100 plastic Petri dishes. The collector was located on the top deck and equipped with a control



101 system to stop pumping when the wind came from a direction greater than 60 ° from the bow
102 to prevent ship smoke collection. To protect the samples from rain, the filter support was angled
103 downwards and covered with a plastic protector. A flow meter provided information on the
104 pumped air flow: 8 L.min⁻¹ for A281 and A284 samples and 28 L.min⁻¹ for the eight other
105 samples. Each sample was collected over a duration of 3 days on average, for sample size
106 ranging between 9 and 93 m³ (from coastal to open ocean areas). The sampling locations are
107 reported in Fig. 1. The sampling area is more than 8,000 km wide.

108



109

110 Figure 1. Location of aerosol samples. Aerosol sampling transects are shown by the thick lines.
111 The Fe isotopic compositions are indicated by the color bar and under the sample names. PNG
112 stands for Papua New Guinea. BS stands for Bismarck Sea.

113

114 Three samples previously published close to the Bismarck Sea and in the Equatorial Pacific are
115 reported to enrich the discussion: A269, A266 and A259 (Fig. 1 and Table 3) (Labatut et al.,
116 2014).

117



118 **2.2. ANALYTICAL PROCEDURE**

119 The elemental concentrations and iron isotopic compositions were measured at LEGOS
120 laboratory (Observatoire Midi-Pyrénées, Toulouse, France), in the years 2009 to 2012. The
121 analytical procedure was described by Labatut et al. (2014) and is summarized here. A trace
122 metal clean laboratory, an ISO4 laminar flow hood, high purity reagents and acid cleaned
123 labware were used for all chemical procedures. The particles were totally digested using a
124 mixture of 5 M HCl, 2.1 M HNO₃ and 0.6 M HF at 130 °C. To check that the procedure was
125 quantitative, some filters were digested a second time and no PFe was detected in the second
126 leach. A ⁵⁷Fe-⁵⁸Fe double spike was added to the leachates. 2 % aliquots were taken for multi-
127 elemental concentration determination on an Element-XR HR-ICP-MS. Na, Mg, Al, Ca, Ti, Fe,
128 V, Zn, Rb, Sr, Ba, La, Ce and Pb concentrations were quantified. Fe was purified from the
129 remaining 98 % with an AG[®] 1-X4 anionic resin, and its isotopic composition and
130 concentration measured on a Neptune MC-ICPMS.

131 Throughout this article, uncertainties are given at a 95 % confidence level. For the Fe
132 concentration and isotope measurements on the Neptune, the total procedural recovery was
133 93 ± 25 %. Total procedural blank was 3.0 ng, which was 3.8 and 14.7 % of the average and
134 smallest sample, respectively. Repeatability was not determined on aerosol samples but was
135 quantified during the same measurement sessions from duplicate analyses, including distinct
136 chemical treatments, of four seawater suspended particle samples. It was 4 % and 0.04 % for
137 concentration and isotopic composition, respectively. This repeatability for $\delta^{56}\text{Fe}$ is better than
138 the long-term external precision of 0.07 ‰ of our measurements, determined from repeated
139 analysis of a secondary isotopic standard (an in-house "hematite" standard). The uncertainties
140 characterizing our Fe isotope data are therefore 0.07 ‰ or the internal measurement uncertainty
141 (2 standard errors), when the latter is larger. The iron isotope protocol at LEGOS has been
142 validated through intercalibration and intercomparison exercises (Boyle et al., 2012; Conway
143 et al., 2016) and described in Lacan et al. (2008, 2010, 2021). Trueness of concentrations



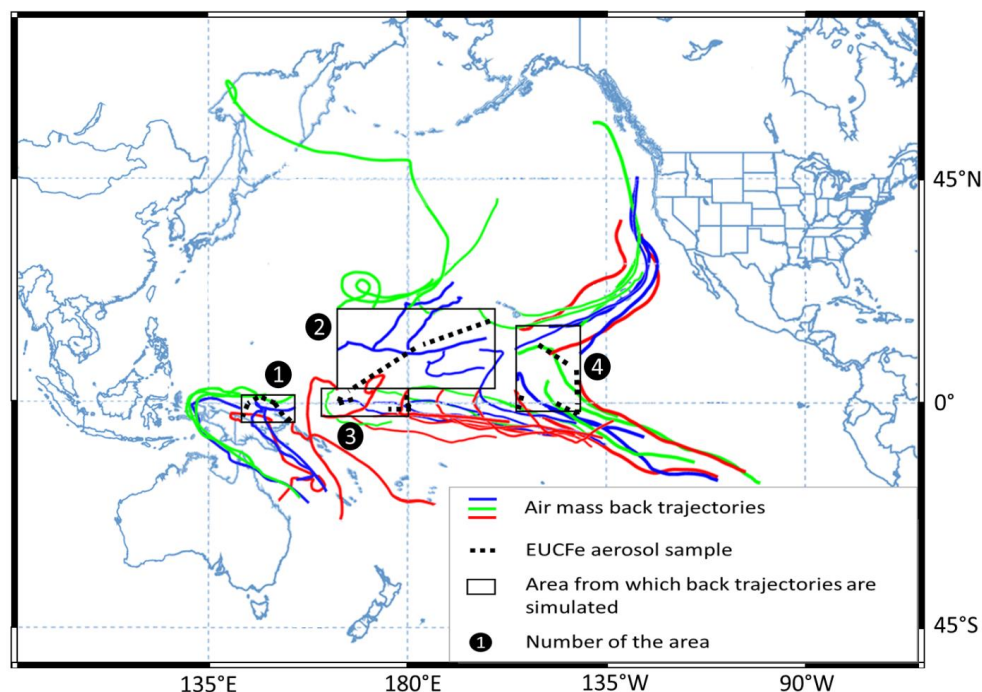
144 determined by HR-ICPMS analysis was verified using certified SLRS-5 river water material.
145 The quality (trueness and repeatability) of our HR-ICPMS concentration determination was
146 also validated through intercalibration exercises (Yeghicheyan et al., 2013, 2019). Based on
147 the measured Fe blank, and assuming a crustal composition for aerosols, blank levels are always
148 lower than 15 % of each sample and all elements, except for Ca for which it was 11.8 % on
149 average and 35.7 % maximum.

150

151 **2.3. HYSPLIT MODEL**

152 To identify the origin of sampled aerosols, air mass back trajectories were calculated
153 using the NOAA Hybrid Single-Particle Lagrangian Integrated Trajectory (HYSPLIT) model
154 (Stein et al., 2015). The meteorological data selected was the Global Data Assimilation System
155 (GDAS). Trajectories were computed at 50 m above ground level with a 7.5 days run time.
156 Aerosol samplings were conducted between 22 August and 12 October 2006. In order to
157 represent spatial and temporal variabilities and to present a synthetic overview, we divided the
158 cruise track in four areas (Fig. 2).

159



160

161 Figure 2. Air mass back trajectories (colors lines) calculated with Hybrid Single-Particle
 162 Lagrangian Integrated Trajectory model (HYSPLIT, NOAA, GDSA Meteorological Data).
 163 Trajectories were conducted at the height of 50 m (AGL) with a 7.5 days run time. Air mass
 164 back trajectories' colors are only used for easier understanding.

165

166 For each area from which back trajectories are simulated, the starting points of back
 167 trajectories were chosen as a grid for representativity and clarity purposes. The grid points are
 168 not precisely sampling locations but they are close to them. The starting times were chosen as
 169 the central dates between the sampling period of each area (Table 1).

170

171 Table 1. Parameters selected for the HYSPLIT model simulations and the aerosol sample names
 172 within areas from which back trajectories are simulated.

Area Number	Area – Lower left grid point	Area – Upper right grid point	Number of starting points within the area	Starting time	Aerosol samples within the area
-------------	------------------------------	-------------------------------	---	---------------	---------------------------------



1	142° E 4° S	154° E 2° N	9	25 September 2006, 16:00:00 UTC	A266, A269
2	164° E 3° N	160° W 21° N	15	11 October 2006, 16:00:00 UTC	A281, A284
3	164° E 3° S	180° 3° N	9	13 September 2006, 16:00:00 UTC	A252, A259
4	155° W 1° S	139° W 15° N	12	26 August 2006, 16:00:00 UTC	A233, A235, A238, A243

173

174

175 3. RESULTS

176 Elemental concentrations are presented in Table 2. Isotopic compositions of Fe in
177 aerosols are reported in Table 3 and in Fig. 1.

178

179 Table 2. Aerosol elemental concentrations from the EUcFe cruise. Concentration uncertainty
180 was 4 % (95 % confidence level). Some concentrations were found below quantification limits.
181 In that case, they are reported after the "<" symbol. The mean concentrations do not take into
182 account samples with concentration below quantification limits. Al concentrations for A252
183 sample (reported in brackets in the table) was suspected to be contaminated, it is not included
184 in the mean calculation and in the discussion. UCC stands for Upper Continental Crust.



Samples	[Na] ng.m ⁻³	[Mg] ng.m ⁻³	[Ca] ng.m ⁻³	[Sr] pg.m ⁻³	[Ba] pg.m ⁻³	[Al] ng.m ⁻³	[Ti] ng.m ⁻³	[V] pg.m ⁻³	[Fe] ng.m ⁻³	[La] pg.m ⁻³	[Ce] pg.m ⁻³	[Zn] pg.m ⁻³	[Rb] pg.m ⁻³	[Pb] pg.m ⁻³
A233	135	17.5	13.4	170	37.4	2.42	0.30	5.91	1.71	0.43	1.20	798	< 22.3	11.1
A235	1 085	128	64.9	1 144	28.2	1.90	0.73	7.09	7.22	0.59	1.78	3 795	13.5	14.4
A238	3 031	323	126	2 169	272	20.3	0.59	13.4	3.81	1.57	4.59	786	58.7	17.2
A243	1 021	114	49.0	730	372	26.1	0.50	< 49.9	2.28	0.99	1.78	1 143	45.5	< 63.2
A252	2 432	223	85.4	1 552	68.2	(188)	0.22	64.9	0.99	0.48	0.71	749	20.5	13.9
A259	809	77.6	36.1	520	< 40.9	0.76	0.20	4.77	0.38	0.68	1.28	624	< 28.8	10.7
A266	224	20	8.93	< 91.4	< 18.6	1.28	0.12	< 12.6	5.56	< 4.15	< 4.21	< 407	< 13.1	< 16.0
A269	121	12.5	4.94	84.6	17.9	2.19	0.11	< 16.6	0.54	0.62	1.17	387	< 17.2	19.9
A281	653	58.6	26.0	373	75.0	9.15	0.42	20.9	2.42	1.24	2.97	795	< 41.1	29.5
A284	1 072	97.7	41.5	652	418	23.5	0.45	28.4	5.17	2.42	8.51	1 633	50.3	41.8
Mean concentrations of samples	1 058	107	45.6	822	161	9.7	0.36	20.8	3.01	1.00	2.66	1 190	38	19.8
Mean UCC in g.g ⁻¹ (Rudnick and Gao, 2014)	2.43 x 10 ⁻²	1.50	2.57	3.20 x 10 ⁻⁴	6.24 x 10 ⁻⁴	8.15 x 10 ⁻²	3.84 x 10 ⁻³	9.70 x 10 ⁻⁵	3.92 x 10 ⁻²	3.10 x 10 ⁻⁵	6.30 x 10 ⁻⁵	6.70 x 10 ⁻⁵	8.40 x 10 ⁻⁵	1.70 x 10 ⁻⁵
Typical North Pacific concentrations in filtered seawater in ng.kg ⁻¹ (Nozaki, 1997)	1.08 x 10 ¹⁰	1.28 x 10 ⁹	4.12 x 10 ⁸	7.80 x 10 ⁶	1.50 x 10 ⁴	30.0	6.50	2.00 x 10 ³	30.0	5.60	0.70	3.50 x 10 ²	1.20 x 10 ⁵	2.70



186 Table 3. Aerosol Fe isotopic compositions during the EUcFe cruise. U95 stands for
187 measurement uncertainty at the 95 % confidence level. (*) identifies data previously published
188 by Labatut et al. (2014).

Samples ID	Location	Sampling date	$\delta^{56}\text{Fe}$ (‰)	$\delta^{56}\text{Fe}$ U95 (‰)
A233	from 12.39° N 149.54° W to 06.01° N 143.42° W	21-23/08/2006	0.14	0.07
A235	from 06.01° N 143.42° W to 01.07° N 140.00° W	23-25/08/2006	0.31	0.07
A238	from 00.0° N 140.0° W to 00.52° S 144.15° W	26-28/08/2006	-0.16	0.07
A243	from 01.02° N 154.60° W to 01.31° S 155.00° W	31/08-01/09/2006	0.43	0.07
A252	from 02.02° N 180.00° E to 01.22° S 178.16° E	09-11/09/2006	0.26	0.07
A259*	from 01.48° N 167.31° E to 01.06° N 164.59° E	16-17/09/2006	0.27	0.15
A266*	from 02.32° S 153.56° E to 01.18° N 146.34° E	23-25/09/2006	0.35	0.07
A269*	from 01.18° N 146.33° E to 03.21° S 143.52° E	26-28/09/2006	0.38	0.08
A281	from 03.39° N 167.55° E to 13.02° N 175.06° W	08-11/10/2006	0.22	0.09
A284	from 14.20° N 173.5° W to 20.20° N 160.50° W	11-14/10/2006	0.47	0.08

189

190 3.1. ELEMENTAL CONCENTRATIONS

191 Aerosol iron concentrations ranged from $0.38 \pm 0.02 \text{ ng.m}^{-3}$ to $7.22 \pm 0.28 \text{ ng.m}^{-3}$
192 (Table 2). Excluding aerosol sample A266 close to the Bismarck Sea ($5.56 \pm 0.22 \text{ ng.m}^{-3}$),
193 concentrations vary from low values ($< 1 \text{ ng.m}^{-3}$) between 140° E and 160° W along the equator
194 to large values ($> 1.5 \text{ ng.m}^{-3}$ and $< 8 \text{ ng.m}^{-3}$) in the North Tropical Pacific region and between
195 160° W and 140° W along the equator. There was no correlation between distance from land and
196 concentration. A major volcanic eruption of Tavurvur (Papua New Guinea) occurred on 7
197 October 2006 (Wunderman, 2006). Samples A233 to A269 were collected prior to this event
198 and are therefore unaffected. While it is theoretically possible that samples A281 and A284
199 could have been influenced by the eruption, they were collected over 1,500 km away from the



200 volcano. Additionally, their concentrations are consistent with those of samples collected before
201 the eruption, confirming that they were not impacted.

202 Aerosols Fe concentrations in EUFe samples are consistent with the literature in the
203 Central Equatorial Pacific for particulate Fe: $2.01 \pm 1.56 \text{ ng.m}^{-3}$ (2SD, n=11) (GEOTRACES
204 GP15 cruise: between 20° N and 20° S and along the 152° W meridian) (Marsay et al., 2022),
205 $5.60 \pm 5.65 \text{ ng.m}^{-3}$ (2SD, n=8) (P16 cruise of the CLIVAR/CO2 Repeat Hydrography Program:
206 between 9° N and 2° S and along the 151° W meridian) (Landing et al., 2013). The range of
207 EUFe values was also similar to concentrations in Alaskan coastal and pelagic regions in the
208 subarctic North Pacific, in the North Pacific and in the South Pacific (Buck et al., 2019; Kurisu
209 et al., 2021, 2024; Marsay et al., 2022; Sakata et al., 2022). EUFe data are lower than aerosol
210 iron concentrations reported in the coastal Northwest Pacific, closer to industrialized areas
211 (Kurisu et al., 2021; Sakata et al., 2022).

212 The concentrations of the major elements of seawater (Na, Mg, Ca, Sr), and by extension
213 of sea spray, depends on the height of sampling, wave height and wind intensity. Thus, there is
214 no interest to compare Na, Mg, Ca and Sr concentrations of EUFe samples with Na, Mg, Ca
215 and Sr concentrations measured in other samples in the Pacific. However, we can compare Al,
216 Ti, V, Zn and Pb elements with the literature. Their concentrations are in the same order of
217 magnitude as those found previously in the atmosphere over the North Pacific (Kurisu et al.,
218 2021, 2024). To the best of our knowledge, the EUFe Rb, Ba, La and Ce concentrations are
219 the first measurements over the Pacific Ocean. Their concentrations are similar to those of
220 aerosols over the Atlantic Ocean (Landing and Shelley, 2014; Shelley et al., 2017).

221 Overall, these comparisons are consistent with previous values for these elements and
222 validate the analytical procedure, from sampling to final concentrations.

223



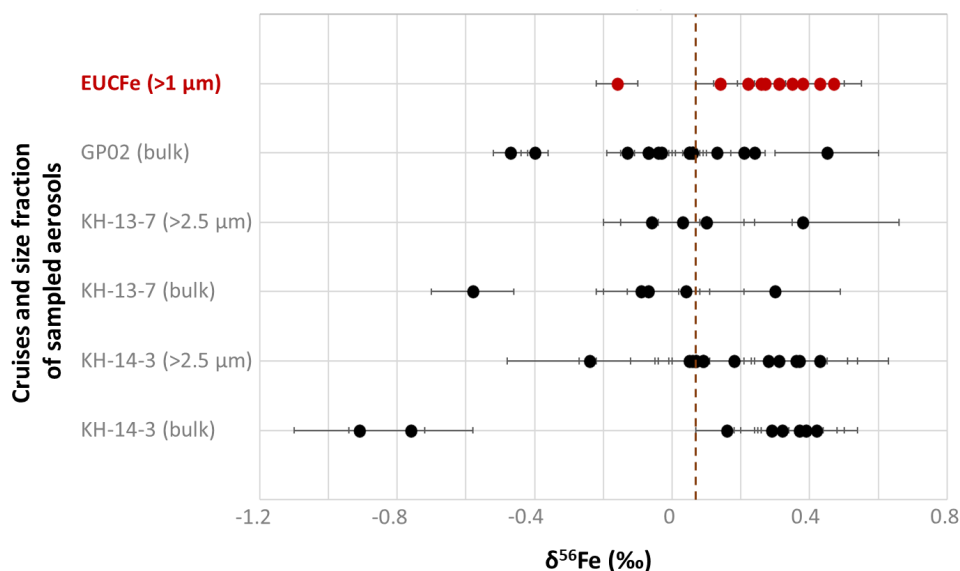
224 **3.2. IRON ISOTOPIC COMPOSITIONS**

225 Aerosols have Fe isotopic ratios ranging from -0.16 ‰ to 0.47 ‰ (Table 3, Fig. 1 and
226 Fig. 3). The aerosols sampled along the equator and close to the Bismarck Sea have similar,
227 slightly heavy, signatures from 0.26 ‰ to 0.43 ‰. Aerosols in the North Tropical Pacific
228 present more variable signatures, but still positive from 0.14 ‰ to 0.47 ‰. One sample, the
229 southeastern most one (A238), differed significantly from the others in the Equatorial Pacific
230 with the lightest value, -0.16 ‰.

231 $\delta^{56}\text{Fe}$ marine aerosols values from the EUCFe cruise can be compared with three other
232 cruises in the Pacific: KH-13-7 and KH-14-3 in the North Pacific (Kurusu et al., 2021) and
233 GP02 in the subarctic North Pacific (Kurusu et al., 2024) (Fig. 3). In these previous studies, all
234 $\delta^{56}\text{Fe}$ values below 0 ‰ were measured in samples taken less than 1,500 km from the Japanese
235 and Alaskan coasts (Fig. 3). In the open ocean, they also reported positive $\delta^{56}\text{Fe}$ values as for
236 EUCFe samples (apart from sample A238). South of the tropic of Cancer, Kurusu et al. (2021)
237 reported bulk aerosols heavy $\delta^{56}\text{Fe}$ values, between 0.04 ‰ and 0.42 ‰ with a mean value of
238 0.27 ± 0.26 ‰ (2SD, n=7). In the subarctic North Pacific, the pelagic and Alaskan areas have
239 $\delta^{56}\text{Fe}$ values between -0.07 ‰ and 0.45 ‰ (Kurusu et al., 2024). Overall, EUCFe $\delta^{56}\text{Fe}$ values
240 are in excellent agreement with these previous works.

241

242



243

244 Figure 3. $\delta^{56}\text{Fe}$ (‰) of sampled aerosols during EUCFe in the Equatorial and Tropical Pacific,
245 GP02 in the subarctic North Pacific (Kurisu et al., 2024), KH-13-7 and KH-14-3 cruises in the
246 North Pacific (Kurisu et al., 2021). Error bars represent 2SD (‰) for EUCFe and GP02 cruises
247 and 2SE (‰) for KH-13-7 and KH-14-3 cruises. 2SE only reflects the dispersions of the MC-
248 ICPMS treatment. The vertical brown line indicates the upper crust value, 0,07 ‰ (Poitrasson,
249 2006).

250

251 4. DISCUSSION

252 All our marine aerosol samples, except the southeastern one (A238), are enriched in
253 heavy isotopes relative to the crustal value. On average those are characterized by
254 $\delta^{56}\text{Fe} \approx 0.31 \pm 0.21$ ‰ (2SD, n=9) (average value except A238, Table 3 and Fig. 1). The value
255 for sample A238 was $\delta^{56}\text{Fe} = -0.16$ ‰.

256

257



258 **4.1. SOURCES SIGNATURES**

259 First, we will discuss the possibility that aerosol signatures correspond to unmodified
260 source signatures. We will explore three hypotheses: contributions i) from sea spray, ii) from
261 crustal sources, iii) from anthropogenic sources.

262 A first hypothesis is a contribution from seawater, i.e., sea spray. Based on the
263 assumptions that all Na in EUCFe samples comes from seawater and that the chemical
264 composition of sea spray is that of North Pacific seawater (Nozaki, 1997), the contribution of
265 sea spray to our samples can be estimated with the following equation (Eq. 2).

266
$$[EI_{\text{Sea-spray}}] = [Na_{\text{sample}}] \frac{[EI_{\text{SW-ref}}]}{[Na_{\text{SW-ref}}]} \quad (2)$$

267 where EI is the element of interest (Fe for instance) and SW-ref is the seawater used as a
268 reference (Nozaki, 1997) for Na and EI.

269 This leads to insignificant contributions ($< 10^{-6}$ %) for Fe for all our samples (Table2).
270 On the other hand, the estimated sea spray contribution for Mg, Ca and Sr was > 89 % for all
271 samples.

272 A second hypothesis is a source from crustal desert or volcanic contribution. Desert
273 dust, e.g., of Saharan origin, displays crustal signatures (Beard et al., 2003; Waeles et al., 2007;
274 Mead et al., 2013; Conway et al., 2019). Ash, originating from active volcanoes around the
275 Bismarck Sea, have not been directly documented to date to our knowledge, but their signature
276 is likely also crustal, since i) runoff water collected from the flanks of volcano Rabaul in the
277 Bismarck area has been characterized by $\delta^{56}\text{Fe} = 0.07 \pm 0.03$ ‰ (2SD, n=2) (Labatut et al.,
278 2014) and ii) basalts also display a crustal signature (Poitrasson, 2006; Craddock et al., 2013;
279 Teng et al., 2013). Therefore, EUCFe aerosol sample isotopic signatures, whether those in the
280 group of nine samples slightly enriched in heavy isotopes or that of the A238 sample slightly
281 enriched in light isotopes, do not directly reflect a crustal source.



282 A third hypothesis is an anthropogenic origin. Human activities emit aerosols within a
283 wide range of $\delta^{56}\text{Fe}$. On the one hand, biomass burning, vehicle exhaust, steel manufacturing,
284 solid waste incineration have been characterized by negative $\delta^{56}\text{Fe}$ signatures (Mead et al.,
285 2013; Kurisu et al., 2016a; Kurisu and Takahashi, 2019). On the other hand, coal fly ash,
286 metallic brake dust and steel manufacturing have been characterized by positive $\delta^{56}\text{Fe}$
287 signatures (Flament et al., 2008; Majestic et al., 2009; Mead et al., 2013; Li et al., 2022).

288 Sample A238 ($\delta^{56}\text{Fe}=-0.16\text{‰}$) is located in the southern part of the Pacific around
289 140° W (Fig. 1 and Fig. 3, Table 3). The air mass back trajectories (Fig. 2) suggest that aerosols
290 collected in this area originated from the South Pacific or the South American coast. As stated
291 above, several anthropogenic sources, biomass burning, vehicle exhaust, steel manufacturing
292 and solid waste incineration have been characterized by negative signatures (Mead et al., 2013;
293 Kurisu, Sakata, et al., 2016; Kurisu & Takahashi, 2019). Combustion processes from South
294 America are therefore a potential explanation for A238 sample.

295 The remaining of the discussion will focus on the group of nine samples, characterized
296 by slightly heavy Fe isotopic composition ($\delta^{56}\text{Fe} = 0.31 \pm 0.21\text{‰}$, 2SD, n=9; Fig. 1 and Fig. 3,
297 Table 3). From a purely isotopic signature point of view, anthropogenic sources, e.g., coal
298 combustion and steel manufacturing, possibly mixed with crustal sources, could explain these
299 slightly heavy signatures (Wei et al., 2024). Nevertheless, there are several arguments
300 contradicting this hypothesis: demography, modeled atmospheric back trajectories, aerosol size
301 ($> 1\ \mu\text{m}$) and elemental ratios such as Fe/Ti. While discussing similar slightly heavy aerosol
302 isotopic signatures in the Bismarck Sea, a possible anthropogenic pollution contribution was
303 excluded (Labatut et al., 2014) given the very low demography of the surroundings lands such
304 as Papua New Guinea (Brunskill, 2004). Back trajectories presented in Fig. 2 reveal that the
305 sampled air masses had a wide variety of geographic origins. The fact that aerosols have
306 variable sources but similar isotope signatures does not support the hypothesis of an
307 anthropogenic source such as coal fly ash, metallic brake dust and steel manufacturing, which



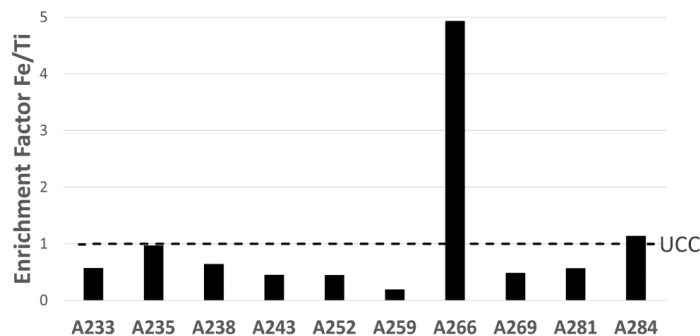
308 are not expected to be widely and homogeneously distributed around our study area. The
309 separation between fine and coarse aerosol particles is 2 μm to 2.5 μm (Whitby, 1978; Seinfeld
310 and Pandis, 2006). Nevertheless, fine particles do not ordinarily grow larger than 1 μm (Whitby,
311 1978). The EUFe samples are mainly coarse aerosols, a size fraction associated with crustal
312 sources (Mead et al., 2013).

313 The enrichment factor (EF) in an element of interest relative to the crust (Zoller et al.,
314 1974) can be defined as (Eq. 3):

$$315 \quad \text{Enrichment Factor (EF)} = \frac{\left(\frac{\text{Element of interest}}{\text{Lithogenic tracer}}\right)_{\text{sample}}}{\left(\frac{\text{Element of interest}}{\text{Lithogenic tracer}}\right)_{\text{UCC}}} \quad (3)$$

316 UCC stands for upper continental crust (Rudnick and Gao, 2014). Ti and Al are often used as
317 lithogenic tracers (Dammshäuser, 2012). Because one sample (A252) is suspected to be
318 contaminated in Al (Table 2), we chose Ti to calculate the EF relative to the crust in the
319 following.

320



321

322 Figure 4. Enrichment factors for Fe relative to Ti.

323

324 The EF for Fe/Ti ranges between 0.19 and 4.93 for all samples (Fig. 4). Samples with
325 EFs below 10 are considered natural, without enrichment from an anthropogenic source



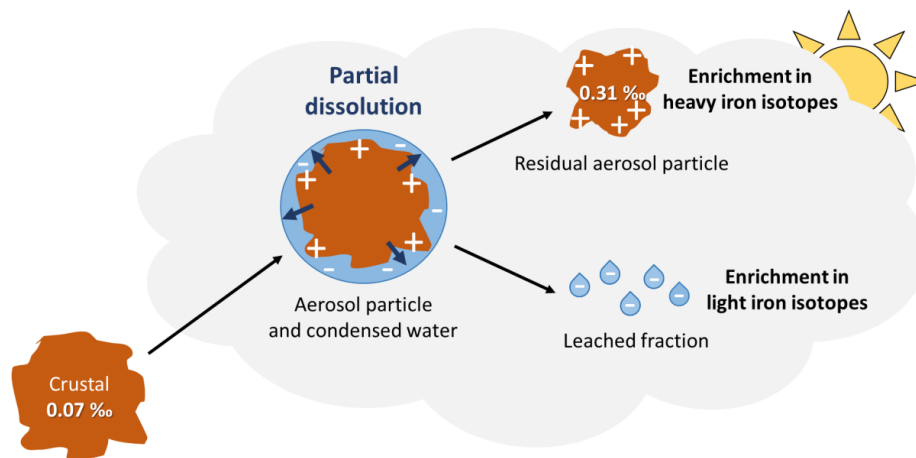
326 (Gelado-Caballero et al., 2012). Based on the assumptions that all Ti in EUFe samples comes
327 from the UCC, and that the chemical composition of crustal aerosol is that of UCC (Rudnick
328 and Gao, 2014), the lithogenic contribution to our samples can be estimated (adjusting Eq. 2 to
329 the case of a lithogenic source). For Fe, this leads to high lithogenic contributions (123 % on
330 average). The fact that this calculation leads to contributions larger than 100 % likely reflects
331 source ratios which differ from that chosen above (UCC) and/or Fe removal during transport.

332 These arguments, suggest that the slightly heavy iron isotopic compositions are not
333 explained by anthropogenic sources, but mainly by crustal ones. We will discuss below if our
334 observations ($\delta^{56}\text{Fe}_{\text{average}} = 0.31 \text{ ‰}$) can be explained by aerosols of crustal origin (0.07 ‰)
335 which isotopic signature has been modified by isotopic fractionation during atmospheric
336 transport.

337 **4.2. ISOTOPIC FRACTIONATION DURING ATMOSPHERIC PROCESSES**

338 A major process influencing aerosol chemistry, during atmospheric transport, is partial
339 dissolution during condensation/evaporation cycles in clouds (Lelieveld and Crutzen, 1991;
340 Desboeufs, 2001). Atmospheric aerosol Fe dissolution is mainly due to dissolution by low pH
341 cloud water and effects of solar irradiation. Proton-promoted, ligand-controlled and reductive
342 ligand-promoted dissolution are mechanisms happening in clouds (Wiederhold et al., 2006;
343 Maters et al., 2022). These processes fractionate iron isotopes (Mulholland et al., 2021; Maters
344 et al., 2022). In most studies, light iron isotopes are preferentially dissolved, and, the isotopic
345 composition of the remaining particulate iron becomes gradually heavier (Maters et al., 2022)
346 (Fig. 5).

347



348 Crustal aerosol particle

349 Figure 5. Path of an aerosol during atmospheric transport undergoing partial dissolution. Partial
350 dissolution and subsequent separation of the leached fraction leads the residual particle to an
351 enrichment in heavy and light iron isotopes, in the particles and leached fraction, respectively.

352

353 The magnitude of the isotope fractionations, $\Delta^{56}\text{Fe}_{\text{solution} - \text{particle}}$, were found between -
354 0.9 and -1.4 ‰ after biotite and chlorite minerals dissolution (Kiczka et al., 2010) and between
355 -0.4 ± 0.2 ‰ and -1.0 ± 0.15 ‰ (apparent steady state values) after granite and basalts
356 dissolution by hydrochloric acid or oxalic acid (Chapman et al., 2009). An experimentation of
357 anthropogenic aerosols dissolution with synthetic cloud water solution showed light $\delta^{56}\text{Fe}$
358 release ($\Delta^{56}\text{Fe}_{\text{solution} - \text{particle}} = -0.284 \pm 0.103$ ‰) in solution within the first hour of dissolution
359 but heavy $\delta^{56}\text{Fe}$ release ($\Delta^{56}\text{Fe}_{\text{solution} - \text{particle}} = 0.227 \pm 0.091$ ‰) in solution after 1 hour
360 (Mulholland et al., 2021). Another experimentation of mineral dust and industrial ash
361 dissolution in simulated cloud water showed a light $\delta^{56}\text{Fe}$ enrichment in solution, $\Delta^{56}\text{Fe}_{\text{solution} -$
362 particle between -0.18 ‰ and -0.66 ‰ for ash and between -0.98 ‰ and -1.18 ‰ for dust (Maters
363 et al., 2022). Thus, mineral dissolution appears to favor light isotopes, thereby enriching the
364 remaining solid fraction in heavy isotopes. Therefore, we will assess whether partial dissolution
365 during clouds transport can produce aerosols with a heavier iron isotopic composition. Some



366 authors have suggested that the observed isotopic compositions may be partly due to isotopic
367 fractionation during transport (Kurisu et al., 2021, 2024; Wang et al., 2022).

368 Considering that the leachate is isolated from the solid fraction of the aerosol, the system
369 can be modeled as a Rayleigh distillation. The isotope composition of the solid fraction of the
370 aerosol is calculated according to Eq. (4) and (5):

$$371 \quad (\delta^{56}\text{Fe}_{\text{particle}})_f \approx (\delta^{56}\text{Fe}_{\text{particle}})_{f=1} + \Delta^{56}\text{Fe}_{\text{solution} - \text{particle}} \ln(f) \quad (4)$$

372 where the particle is the solid fraction of the aerosol, the solution is the leached solution and f
373 is the remaining fraction of $\text{Fe}_{\text{particle}}$ (when $f = 1$ all Fe is in the particle; no Fe has been leached).

374 For the particle value, we assume an initial crustal signature for EUCCa aerosols,
375 $(\delta^{56}\text{Fe}_{\text{particle}})_{f=1} = 0.07 \text{ ‰}$ (Poitrasson, 2006). For the isotopic fractionation, $\Delta^{56}\text{Fe}_{\text{solution} - \text{particle}}$,
376 although the experiments described above observed, values ranging between -1.4 and 0.23 ‰,
377 we choose -1.1 ‰ (Maters et al., 2022). This value was measured during a laboratory
378 experiment on dust with simulated cloud water, i.e., a similar situation to the EUCCa field study
379 (Maters et al., 2022). Equation 5 (derived from Eq. 4) allows us to estimate the fractions of the
380 particles that have to be dissolved (1-f) in order reach the slightly heavy isotope composition
381 measured.

$$382 \quad 1 - f = 1 - e^{\frac{(\delta^{56}\text{Fe}_{\text{particle}})_{f=1} - (\delta^{56}\text{Fe}_{\text{particle}})_f}{\Delta^{56}\text{Fe}_{\text{solution} - \text{particle}}}} \quad (5)$$

383 Based on these calculations, we estimate Fe dissolution percentages varying from 6 to
384 30 % with an average value of 20 % (Table 4). This is the first estimate of this kind to our
385 knowledge. A comparison can be made with Fe fractional solubility of aerosols measured
386 during seawater or ultrapure deionized water leaching experiments (Sholkovitz et al., 2012;
387 Buck et al., 2013; Shelley et al., 2018; Kurisu et al., 2021, 2024; Desboeufs et al., 2024),
388 keeping in mind that clouds are slightly acidic with a pH around 5 in the Equatorial Pacific
389 (Shah et al., 2020). Locally, Fe fractional solubility can reach 52 % in the subarctic North



390 Pacific (Kurusu et al., 2024), 23 % in the Northwestern Pacific (Kurusu et al., 2021), 29 % in
391 the Pacific Ocean (3 cruises) (Buck et al., 2013) during leaching experiments with ultrapure
392 deionized water. Mean Fe fractional solubility has been reported as the highest in the world in
393 the Equatorial Pacific, with mean values ranging from 12 to 20 % (Hamilton et al., 2019). Fe
394 fractional solubility depends on numerous factors such as aerosols size and origin, atmospheric
395 processes (pH, solar irradiation, composition of the solution). Crustal aerosols collected during
396 dust events in coastal Namibia (aerosols < 10 μm), can reach high Fe fractional solubilities of
397 20 % (Desboeufs et al., 2024). Therefore, a 20 % dissolution is a rather high value for crustal
398 aerosols, but is realistic.

399

400 Table 4. Percentage of Fe dissolution (1-f) necessary to explain the observed EUCFe $\delta^{56}\text{Fe}$
401 through atmospheric isotopic fractionation from initial isotope signature of the upper crust
402 (0.07 ‰). Calculations are performed for all our samples except A238.

Samples	$(\delta^{56}\text{Fe}_{\text{particle}})_f$ (‰)	1-f (%)
A233	0,14	6
A235	0,31	20
A281	0,22	13
A284	0,47	30
A243	0,43	28
A252	0,26	16
A259	0,27	17
A266	0,35	22
A269	0,38	25
Average of all the above samples	0.31	20

403

404



405 An isotopic fractionation by partial dissolution of crustal origin aerosols could therefore
406 explain the slightly heavy signatures observed (Fig. 5). This would require that the leached
407 fraction, enriched in light isotopes, is separated from the solid fraction. In the absence of
408 separation, the effect of isotope fractionation would not have been measured in our samples.
409 This process has not yet been demonstrated, but the hypothesis has already been proposed in
410 two publications (Kurisu et al., 2021, 2024). The processes that could lead to such separation
411 are difficult to identify. They are however necessary to explain our observations provided that
412 the anthropogenic hypothesis has been rejected. Shattering or ice-breaking are two ways to
413 separate the leached fraction and the residual particle of the aerosols. Their occurrence is
414 understudied especially regarding shattering process. The above model considers the aerosol
415 as a bulk, a homogeneous reservoir. In reality, fractionation occurs at the surface. Taking into
416 account surface processes, would lead to smaller isotopic effects (Wiederhold et al., 2006). Our
417 approximation led to an overestimation of the effect of isotope fractionation and therefore an
418 underestimation of the leached fraction.

419

420 **5. CONCLUSION**

421 Fe isotope compositions ($\delta^{56}\text{Fe}$) and elemental concentrations (Na, Mg, Al, Ca, Ti, Fe,
422 V, Zn, Rb, Sr, Ba, La, Ce and Pb) were analyzed in atmospheric particles collected during the
423 EUCFe expedition, in the Equatorial and Tropical Pacific, between Hawaii, the Equator and
424 Papua New Guinea. In all marine aerosol samples with one exception, Fe is enriched in heavy
425 isotopes relative to the crustal value, with an average $\delta^{56}\text{Fe}$ value of 0.31 ± 0.21 ‰ (2SD, n=9).
426 The simulation of air mass back trajectories, the size of particles, their chemical composition
427 compared to potential sources (enrichment factors) and the geographic environment were used
428 to help explain the enrichment in heavy Fe isotopes. An anthropogenic origin was ruled out due
429 to i) the homogeneity aerosols delta values despite a wide variety of modeled geographic origin
430 and ii) the aerosol chemical composition. We conclude that these observations are best



431 explained by crustal aerosols with an initial isotope signature ($\delta^{56}\text{Fe} = 0.07\%$) modified during
432 atmospheric transport by partial dissolution followed by the removal of the leached fraction.
433 Although such removal had not been previously reported, such Fe isotopes fractionation has
434 been documented in controlled experiments (Mulholland et al., 2021; Maters et al., 2022;) and
435 has already been suggested as one of several explanations for *in situ* data (Kurusu et al., 2021,
436 2024). The extent of Fe isotopes fractionation during atmospheric transport requires the
437 dissolution and removal of 6 to 30 % – 20 % on average – of the initial aerosol Fe contents.

438 One aerosol sample stands out by a slightly light isotopic composition of -0.16% ,
439 possibly emitted from combustion processes in South America.

440 This highlights the challenging use of iron isotopes to trace the origin of the aerosols. It
441 also highlights the unique and strong constrains brought by these isotopes on the Fe cycle in
442 atmospheric aerosols. Further studies are needed to confirm the main conclusion of this study,
443 namely the existence of processes leading to the removal of a significant fraction of the iron
444 content of atmospheric aerosols during atmospheric transport.

445

446 **Authors contributions**

447 J.W.M. was the principal investigator of the EUcFe cruise. F.L. conceived the iron
448 isotope work. A.J. supervised the aerosol collection. M.L., C.P. and FL analyzed the samples.
449 C.C. and F.L. wrote the article. All co-authors reviewed the manuscript.

450

451 **Competing interests**

452 The authors declare that they have no conflict of interest.

453



454 **Acknowledges**

455 A Radic is very much thanked for having carried out a part of the isotope work. L. Shank
456 is deeply thanked for having carried out the aerosol sampling on board. J. Chmeleff, F.
457 Candaudap, and A. Marquet are thanked for their support with the ICP-MS at the *Observatoire*
458 *Midi-Pyrénées*. The captain and the crew of the R/V *Kilo Moana* and especially the marine
459 technicians G. Foreman, and D. Fitzgerald are greatly acknowledged.

460

461 **Financial support**

462 This study was funded by French and USA public funds. The CNRS (French National
463 Center for Scientific Research) and the University of Toulouse (France) are thanked. The
464 EUCFe expedition on the R/V *Kilo Moana* was supported by NSF OCE 0425721 (USA). The
465 Fe isotope project was funded par CNRS-INSU ISOFERIX project.

466

467 **References**

- 468 Abadie, C., Lacan, F., Radic, A., Pradoux, C., and Poitrasson, F.: Iron isotopes reveal distinct dissolved
469 iron sources and pathways in the intermediate versus deep Southern Ocean, *Proceedings of the*
470 *National Academy of Sciences*, 114, 858–863, <https://doi.org/10.1073/pnas.1603107114>, 2017.
- 471 Beard, B. L., Johnson, C. M., Von Damm, K. L., and Poulson, R. L.: Iron isotope constraints on Fe
472 cycling and mass balance in oxygenated Earth oceans, *Geology*, 31, 629–632,
473 [https://doi.org/10.1130/0091-7613\(2003\)031<0629:ICOFC>2.0.CO;2](https://doi.org/10.1130/0091-7613(2003)031<0629:ICOFC>2.0.CO;2), 2003.
- 474 Boyd, P. W. and Ellwood, M. J.: The biogeochemical cycle of iron in the ocean, *Nature Geosci*, 3, 675–
475 682, <https://doi.org/10.1038/ngeo964>, 2010.
- 476 Boyle, E. A., John, S., Abouchami, W., Adkins, J. F., Echevoyen-Sanz, Y., Ellwood, M., Flegal, A. R.,
477 Fornace, K., Gallon, C., Galer, S., Gault-Ringold, M., Lacan, F., Radic, A., Rehkamper, M., Rouxel, O.,
478 Sohrin, Y., Stirling, C., Thompson, C., Vance, D., Xue, Z., and Zhao, Y.: GEOTRACES IC1 (BATS)
479 contamination-prone trace element isotopes Cd, Fe, Pb, Zn, Cu, and Mo intercalibration, *Limno*
480 *Oceanogr-Meth*, 10, 653–665, <https://doi.org/10.4319/lom.2012.10.653>, 2012.
- 481 Brunskill, G. J.: New Guinea and its coastal seas, a testable model of wet tropical coastal processes:
482 an introduction to Project TROPICS, *Cont Shelf Res*, 24, 2273–2295,
483 <https://doi.org/10.1016/j.csr.2004.08.001>, 2004.



- 484 Buck, C. S., Landing, W. M., and Resing, J.: Pacific Ocean aerosols: Deposition and solubility of iron,
485 aluminum, and other trace elements, *Mar Chem*, 157, 117–130,
486 <https://doi.org/10.1016/j.marchem.2013.09.005>, 2013.
- 487 Buck, C. S., Aguilar-Islas, A., Marsay, C., Kadko, D., and Landing, W. M.: Trace element concentrations,
488 elemental ratios, and enrichment factors observed in aerosol samples collected during the US
489 GEOTRACES eastern Pacific Ocean transect (GP16), *Chem Geol*, 511, 212–224,
490 <https://doi.org/10.1016/j.chemgeo.2019.01.002>, 2019.
- 491 Chapman, J. B., Weiss, D. J., Shan, Y., and Lemburger, M.: Iron isotope fractionation during leaching
492 of granite and basalt by hydrochloric and oxalic acids, *Geochim Cosmochim Acta*, 73, 1312–1324,
493 <https://doi.org/10.1016/j.gca.2008.11.037>, 2009.
- 494 Conway, T. M. and John, S. G.: Quantification of dissolved iron sources to the North Atlantic Ocean,
495 *Nature*, 511, 212–215, <https://doi.org/10.1038/nature13482>, 2014.
- 496 Conway, T. M., John, S. G., and Lacan, F.: Intercomparison of dissolved iron isotope profiles from
497 reoccupation of three GEOTRACES stations in the Atlantic Ocean, *Mar Chem*, 183, 50–61,
498 <https://doi.org/10.1016/j.marchem.2016.04.007>, 2016.
- 499 Conway, T. M., Hamilton, D. S., Shelley, R. U., Aguilar-Islas, A. M., Landing, W. M., Mahowald, N. M.,
500 and John, S. G.: Tracing and constraining anthropogenic aerosol iron fluxes to the North Atlantic
501 Ocean using iron isotopes, *Nat Commun*, 10, 2628, <https://doi.org/10.1038/s41467-019-10457-w>,
502 2019.
- 503 Craddock, P. R., Warren, J. M., and Dauphas, N.: Abyssal peridotites reveal the near-chondritic Fe
504 isotopic composition of the Earth, *Earth Planet Sc Lett*, 365, 63–76,
505 <https://doi.org/10.1016/j.epsl.2013.01.011>, 2013.
- 506 Dammschäuser, A.: Distribution and behavior of the lithogenic tracers aluminium and titanium in the
507 upper water column of the Atlantic Ocean, Faculty of Mathematics and Natural Sciences Christian-
508 Albrechts-Universität zu Kiel, 2012.
- 509 Desboeufs, K.: Processus de dissolution des aérosols atmosphériques au sein des gouttes d'eau
510 nuageuses, Université Paris-Diderot - Paris VII, 2001.
- 511 Desboeufs, K., Formenti, P., Torres-Sánchez, R., Schepanski, K., Chaboureaud, J.-P., Andersen, H.,
512 Cermak, J., Feuerstein, S., Laurent, B., Klopper, D., Namwoonde, A., Cazaunau, M., Chevaillier, S.,
513 Feron, A., Mirande-Bret, C., Triquet, S., and Piketh, S. J.: Fractional solubility of iron in mineral dust
514 aerosols over coastal Namibia: a link to marine biogenic emissions?, *Atmos Chem Phys*, 24, 1525–
515 1541, <https://doi.org/10.5194/acp-24-1525-2024>, 2024.
- 516 Duce, R. A. and Tindale, N. W.: Atmospheric transport of iron and its deposition in the ocean, *Limnol*
517 *Oceanogr*, 36, 1715–1726, <https://doi.org/10.4319/lo.1991.36.8.1715>, 1991.
- 518 Elrod, V. A., Berelson, W. M., Coale, K. H., and Johnson, K. S.: The flux of iron from continental shelf
519 sediments: A missing source for global budgets, *Geophys Res Lett*, 31,
520 <https://doi.org/10.1029/2004GL020216>, 2004.
- 521 Flament, P., Mattielli, N., Aimo, L., Choël, M., Deboudt, K., Jong, J. de, Rimetz-Planchon, J., and Weis,
522 D.: Iron isotopic fractionation in industrial emissions and urban aerosols, *Chemosphere*, 73, 1793–
523 1798, <https://doi.org/10.1016/j.chemosphere.2008.08.042>, 2008.
- 524 Gelado-Caballero, M. D., López-García, P., Prieto, S., Patey, M. D., Collado, C., and Hernández-Brito, J.
525 J.: Long-term aerosol measurements in Gran Canaria, Canary Islands: Particle concentration, sources



- 526 and elemental composition, *J Geophys Res-Atmos*, 117, <https://doi.org/10.1029/2011JD016646>,
527 2012.
- 528 Hamilton, D. S., Scanza, R. A., Feng, Y., Guinness, J., Kok, J. F., Li, L., Liu, X., Rathod, S. D., Wan, J. S.,
529 Wu, M., and Mahowald, N. M.: Improved methodologies for Earth system modelling of atmospheric
530 soluble iron and observation comparisons using the Mechanism of Intermediate complexity for
531 Modelling Iron (MIMI v1.0), *Geosci Model Dev*, 12, 3835–3862, <https://doi.org/10.5194/gmd-12-3835-2019>, 2019.
- 533 Jickells, T., An, Z., Andersen, K., Baker, A., Bergametti, G., Brooks, N., Cao, J., Boyd, P., Duce, R.,
534 Hunter, K., Kawahata, H., Kubilay, N., Laroche, J., Liss, P., Mahowald, N., Prospero, J., Ridgwell, A.,
535 Tegen, I., and Torres, R.: Global Iron Connections Between Desert Dust, Ocean Biogeochemistry, and
536 Climate, *Science (New York, N.Y.)*, 308, 67–71, <https://doi.org/10.1126/science.1105959>, 2005.
- 537 John, S. G., Mendez, J., Moffett, J., and Adkins, J.: The flux of iron and iron isotopes from San Pedro
538 Basin sediments, *Geochim Cosmochim Ac*, 93, 14–29, <https://doi.org/10.1016/j.gca.2012.06.003>,
539 2012.
- 540 Kiczka, M., Wiederhold, J. G., Frommer, J., Kraemer, S. M., Bourdon, B., and Kretzschmar, R.: Iron
541 isotope fractionation during proton- and ligand-promoted dissolution of primary phyllosilicates,
542 *Geochim Cosmochim Ac*, 74, 3112–3128, <https://doi.org/10.1016/j.gca.2010.02.018>, 2010.
- 543 Klar, J. K., Schlosser, C., Milton, J. A., Woodward, E. M. S., Lacan, F., Parkinson, I. J., Achterberg, E. P.,
544 and James, R. H.: Sources of dissolved iron to oxygen minimum zone waters on the Senegalese
545 continental margin in the tropical North Atlantic Ocean: Insights from iron isotopes, *Geochim
546 Cosmochim Ac*, 236, 60–78, <https://doi.org/10.1016/j.gca.2018.02.031>, 2018.
- 547 Kommalapati, R. R. and Valsaraj, K. T.: Atmospheric Aerosols and Their Importance, in: *Atmospheric
548 Aerosols*, vol. 1005, American Chemical Society, 1–10, <https://doi.org/10.1021/bk-2009-1005.ch001>,
549 2009.
- 550 Kurisu, M. and Takahashi, Y.: Testing Iron Stable Isotope Ratios as a Signature of Biomass Burning,
551 *Atmosphere-Basel*, 10, 76, <https://doi.org/10.3390/atmos10020076>, 2019.
- 552 Kurisu, M., Sakata, K., Miyamoto, C., Takaku, Y., Iizuka, T., and Takahashi, Y.: Variation of Iron Isotope
553 Ratios in Anthropogenic Materials Emitted through Combustion Processes, *Chem. Lett.*, 45, 970–972,
554 <https://doi.org/10.1246/cl.160451>, 2016a.
- 555 Kurisu, M., Takahashi, Y., Iizuka, T., and Uematsu, M.: Very low isotope ratio of iron in fine aerosols
556 related to its contribution to the surface ocean, *J Geophys Res-Atmos*, 121, 11,119–11,136,
557 <https://doi.org/10.1002/2016JD024957>, 2016b.
- 558 Kurisu, M., Sakata, K., Uematsu, M., Ito, A., and Takahashi, Y.: Contribution of combustion Fe in
559 marine aerosols over the northwestern Pacific estimated by Fe stable isotope ratios, *Atmos Chem
560 Phys*, 21, 16027–16050, <https://doi.org/10.5194/acp-21-16027-2021>, 2021.
- 561 Kurisu, M., Sakata, K., Nishioka, J., Obata, H., Conway, T. M., Hunt, H. R., Sieber, M., Suzuki, K.,
562 Kashiwabara, T., Kubo, S., Takada, M., and Takahashi, Y.: Source and fate of atmospheric iron
563 supplied to the subarctic North Pacific traced by stable iron isotope ratios, *Geochim Cosmochim Ac*,
564 378, 168–185, <https://doi.org/10.1016/j.gca.2024.06.009>, 2024.
- 565 Labatut, M., Lacan, F., Pradoux, C., Chmeleff, J., Radic, A., Murray, J. W., Poitrasson, F., Johansen, A.
566 M., and Thil, F.: Iron sources and dissolved-particulate interactions in the seawater of the Western
567 Equatorial Pacific, iron isotope perspectives, *Global Biogeochem Cy*, 28, 1044–1065,
568 <https://doi.org/10.1002/2014GB004928>, 2014.



- 569 Lacan, F., Radic, A., Jeandel, C., Poitrasson, F., Sarthou, G., Pradoux, C., and Freyrier, R.:
570 Measurement of the isotopic composition of dissolved iron in the open ocean, *Geophys Res Lett*, 35,
571 L24610, <https://doi.org/10.1029/2008GL035841>, 2008.
- 572 Lacan, F., Radic, A., Labatut, M., Jeandel, C., Poitrasson, F., Sarthou, G., Pradoux, C., Chmeleff, J., and
573 Freyrier, R.: High-Precision Determination of the Isotopic Composition of Dissolved Iron in Iron
574 Depleted Seawater by Double Spike Multicollector-ICPMS, *Anal. Chem.*, 82, 7103–7111,
575 <https://doi.org/10.1021/ac1002504>, 2010.
- 576 Lacan, F., Artigue, L., Klar, J. K., Pradoux, C., Chmeleff, J., and Freyrier, R.: Interferences and Matrix
577 Effects on Iron Isotopic Composition Measurements by ^{57}Fe - ^{58}Fe Double-Spike Multi-Collector
578 Inductively Coupled Plasma Mass Spectrometry; the Importance of Calcium and Aluminum
579 Interferences, *Front Environ Chem*, 2, <https://doi.org/10.3389/fenvc.2021.692025>, 2021.
- 580 Landing, W. M. and Shelley, R.: Total aerosol trace metal concentrations from R/V Knorr cruises
581 KN199-04 and KN204-01 in the Subtropical northern Atlantic Ocean from 2010-2011 (U.S.
582 GEOTRACES NAT project) (Version 16 September 2014), <http://lod.bco-dmo.org/id/dataset/3865>,
583 2014.
- 584 Landing, W. M., Measures, C. I., and Resing, J. A.: Collaborative Research: Global Ocean Survey of
585 Dissolved Iron and Aluminum and Aerosol Iron and Aluminum Solubility Supporting the Repeat
586 Hydrography (CO₂) Project (CLIVAR AEROSOL) (Version 12 June 2013), 2013.
- 587 Lelieveld, J. and Crutzen, P. J.: The role of clouds in tropospheric photochemistry, *J Atmos Chem*, 12,
588 229–267, <https://doi.org/10.1007/BF00048075>, 1991.
- 589 Li, R., Zhang, H., Wang, F., He, Y., Huang, C., Luo, L., Dong, S., Jia, X., and Tang, M.: Mass fractions,
590 solubility, speciation and isotopic compositions of iron in coal and municipal waste fly ash, *Sci Total*
591 *Environ*, 838, 155974, <https://doi.org/10.1016/j.scitotenv.2022.155974>, 2022.
- 592 Majestic, B. J., Anbar, A. D., and Herckes, P.: Elemental and iron isotopic composition of aerosols
593 collected in a parking structure, *Sci Total Environ*, 407, 5104–5109,
594 <https://doi.org/10.1016/j.scitotenv.2009.05.053>, 2009.
- 595 Marsay, C. M., Kadko, D., Landing, W. M., and Buck, C. S.: Bulk Aerosol Trace Element Concentrations
596 and Deposition Fluxes During the U.S. GEOTRACES GP15 Pacific Meridional Transect, *Global*
597 *Biogeochem Cy*, 36, e2021GB007122, <https://doi.org/10.1029/2021GB007122>, 2022.
- 598 Martin, J. H.: Iron as a Limiting Factor in Oceanic Productivity, in: *Primary Productivity and*
599 *Biogeochemical Cycles in the Sea*, edited by: Falkowski, P. G., Woodhead, A. D., and Vivirito, K.,
600 Springer, Boston, MA, 123–137, https://doi.org/10.1007/978-1-4899-0762-2_8, 1992.
- 601 Maters, E. C., Mulholland, D. S., Flament, P., de Jong, J., Mattielli, N., Deboudt, K., Dhont, G., and
602 Bychkov, E.: Laboratory study of iron isotope fractionation during dissolution of mineral dust and
603 industrial ash in simulated cloud water, *Chemosphere*, 299, 134472,
604 <https://doi.org/10.1016/j.chemosphere.2022.134472>, 2022.
- 605 Mead, C., Herckes, P., Majestic, B. J., and Anbar, A. D.: Source apportionment of aerosol iron in the
606 marine environment using iron isotope analysis, *Geophys Res Lett*, 40, 5722–5727,
607 <https://doi.org/10.1002/2013GL057713>, 2013.
- 608 Moore, J. K. and Braucher, O.: Sedimentary and mineral dust sources of dissolved iron to the world
609 ocean, *Biogeosciences*, 5, 631–656, <https://doi.org/10.5194/bg-5-631-2008>, 2008.
- 610 Morel, F. M. M., Lam, P. J., and Saito, M. A.: Trace Metal Substitution in Marine Phytoplankton, *Annu*
611 *Rev Earth Pl Sc*, 48, 491–517, <https://doi.org/10.1146/annurev-earth-053018-060108>, 2020.



- 612 Mulholland, D. S., Flament, P., de Jong, J., Mattioli, N., Deboudt, K., Dhont, G., and Bychkov, E.: In-
613 cloud processing as a possible source of isotopically light iron from anthropogenic aerosols: New
614 insights from a laboratory study, *Atmos Environ*, 259, 118505,
615 <https://doi.org/10.1016/j.atmosenv.2021.118505>, 2021.
- 616 Nozaki, Y.: A fresh look at element distribution in the North Pacific Ocean, *Eos, Transactions*
617 *American Geophysical Union*, 78, 221–221, <https://doi.org/10.1029/97EO00148>, 1997.
- 618 Poitrasson, F.: On the iron isotope homogeneity level of the continental crust, *Chem Geol*, 235, 195–
619 200, <https://doi.org/10.1016/j.chemgeo.2006.06.010>, 2006.
- 620 Poulton, S. W. and Raiswell, R.: The low-temperature geochemical cycle of iron: From continental
621 fluxes to marine sediment deposition, *Am J Sci*, 302, 774–805, <https://doi.org/10.2475/ajs.302.9.774>,
622 2002.
- 623 Radic, A., Lacan, F., and Murray, J. W.: Iron isotopes in the seawater of the equatorial Pacific Ocean:
624 New constraints for the oceanic iron cycle, *Earth Planet Sc Lett*, 306, 1–10,
625 <https://doi.org/10.1016/j.epsl.2011.03.015>, 2011.
- 626 Raiswell, R., Benning, L. G., Tranter, M., and Tulaczyk, S.: Bioavailable iron in the Southern Ocean: the
627 significance of the iceberg conveyor belt, *Geochem T*, 9, 7, <https://doi.org/10.1186/1467-4866-9-7>,
628 2008.
- 629 Resing, J. A., Sedwick, P. N., German, C. R., Jenkins, W. J., Moffett, J. W., Sohst, B. M., and Tagliabue,
630 A.: Basin-scale transport of hydrothermal dissolved metals across the South Pacific Ocean, *Nature*,
631 523, 200–203, <https://doi.org/10.1038/nature14577>, 2015.
- 632 Rudnick, R. L. and Gao, S.: 4.1 - Composition of the Continental Crust, in: *Treatise on Geochemistry*
633 (Second Edition), edited by: Holland, H. D. and Turekian, K. K., Elsevier, Oxford, 1–51,
634 <https://doi.org/10.1016/B978-0-08-095975-7.00301-6>, 2014.
- 635 Sakata, K., Kurisu, M., Takeichi, Y., Sakaguchi, A., Tanimoto, H., Tamenori, Y., Matsuki, A., and
636 Takahashi, Y.: Iron (Fe) speciation in size-fractionated aerosol particles in the Pacific Ocean: The role
637 of organic complexation of Fe with humic-like substances in controlling Fe solubility, *Atmos Chem*
638 *Phys*, 22, 9461–9482, <https://doi.org/10.5194/acp-22-9461-2022>, 2022.
- 639 Seinfeld, J. H. and Pandis, S. N.: *Atmospheric Chemistry and Physics: From Air Pollution to Climate*
640 *Change*, John Wiley & Sons, 2006.
- 641 Shah, V., Jacob, D. J., Moch, J. M., Wang, X., and Zhai, S.: Global modeling of cloud water acidity,
642 precipitation acidity, and acid inputs to ecosystems, *Atmos Chem Phys*, 20, 12223–12245,
643 <https://doi.org/10.5194/acp-20-12223-2020>, 2020.
- 644 Shelley, R. U., Roca-Martí, M., Castrillejo, M., Sanial, V., Masqué, P., Landing, W. M., van Beek, P.,
645 Planquette, H., and Sarthou, G.: Quantification of trace element atmospheric deposition fluxes to the
646 Atlantic Ocean (>40°N; GEOVIDE, GEOTRACES GA01) during spring 2014, *Deep Sea Research Part I:*
647 *Oceanographic Research Papers*, 119, 34–49, <https://doi.org/10.1016/j.dsr.2016.11.010>, 2017.
- 648 Shelley, R. U., Landing, W. M., Ussher, S. J., Planquette, H., and Sarthou, G.: Regional trends in the
649 fractional solubility of Fe and other metals from North Atlantic aerosols (GEOTRACES cruises GA01
650 and GA03) following a two-stage leach, *Biogeosciences*, 15, 2271–2288, <https://doi.org/10.5194/bg-15-2271-2018>, 2018.
- 652 Sholkovitz, E. R., Sedwick, P. N., Church, T. M., Baker, A. R., and Powell, C. F.: Fractional solubility of
653 aerosol iron: Synthesis of a global-scale data set, *Geochim Cosmochim Ac*, 89, 173–189,
654 <https://doi.org/10.1016/j.gca.2012.04.022>, 2012.



- 655 Stein, A. F., Draxler, R. R., Rolph, G. D., Stunder, B. J. B., Cohen, M. D., and Ngan, F.: NOAA's HYSPLIT
656 Atmospheric Transport and Dispersion Modeling System, *B Am Meteorol Soc*, 96, 2059–2077,
657 <https://doi.org/10.1175/BAMS-D-14-00110.1>, 2015.
- 658 Tagliabue, A., Bopp, L., Dutay, J.-C., Bowie, A. R., Chever, F., Jean-Baptiste, P., Bucciarelli, E., Lannuzel,
659 D., Remenyi, T., Sarthou, G., Aumont, O., Gehlen, M., and Jeandel, C.: Hydrothermal contribution to
660 the oceanic dissolved iron inventory, *Nature Geosci*, 3, 252–256, <https://doi.org/10.1038/ngeo818>,
661 2010.
- 662 Teng, F.-Z., Dauphas, N., Huang, S., and Marty, B.: Iron isotopic systematics of oceanic basalts,
663 *Geochim Cosmochim Acta*, 107, 12–26, <https://doi.org/10.1016/j.gca.2012.12.027>, 2013.
- 664 Waeles, M., Baker, A. R., Jickells, T., and Hoogewerff, J.: Global dust teleconnections: aerosol iron
665 solubility and stable isotope composition, *Environ Chem*, 4, 233, <https://doi.org/10.1071/EN07013>,
666 2007.
- 667 Wang, Y., Wu, L., Hu, W., Li, W., Shi, Z., Harrison, R. M., and Fu, P.: Stable iron isotopic composition of
668 atmospheric aerosols: An overview, *npj Clim Atmos Sci*, 5, 1–13, [https://doi.org/10.1038/s41612-](https://doi.org/10.1038/s41612-022-00299-7)
669 [022-00299-7](https://doi.org/10.1038/s41612-022-00299-7), 2022.
- 670 Wei, T., Dong, Z., Zong, C., Liu, X., Kang, S., Yan, Y., and Ren, J.: Global-scale constraints on the origins
671 of aerosol iron using stable iron isotopes: A review, *Earth-Sci Rev*, 258, 104943,
672 <https://doi.org/10.1016/j.earscirev.2024.104943>, 2024.
- 673 Whitby, K. T.: The physical characteristics of sulfur aerosols, *Atmos Environ*, 12, 135–159,
674 [https://doi.org/10.1016/0004-6981\(78\)90196-8](https://doi.org/10.1016/0004-6981(78)90196-8), 1978.
- 675 Wiederhold, J. G., Kraemer, S. M., Teutsch, N., Borer, P. M., Halliday, A. N., and Kretzschmar, R.: Iron
676 Isotope Fractionation during Proton-Promoted, Ligand-Controlled, and Reductive Dissolution of
677 Goethite, *Environ. Sci. Technol.*, 40, 3787–3793, <https://doi.org/10.1021/es052228y>, 2006.
- 678 Wunderman, R.: Report on Rabaul (Papua New Guinea), *Bulletin of the Global Volcanism Network*,
679 31, <https://doi.org/10.5479/si.GVP.BGVN200609-252140>, 2006.
- 680 Yeghicheyan, D., Bossy, C., Bouhnik Le Coz, M., Douchet, C., Granier, G., Heimbürger, A., Lacan, F.,
681 Lanzaova, A., Rousseau, T. C. C., Seidel, J.-L., Tharaud, M., Candaudap, F., Chmeleff, J., Cloquet, C.,
682 Delpoux, S., Labatut, M., Losno, R., Pradoux, C., Sivry, Y., and Sonke, J. E.: A Compilation of Silicon,
683 Rare Earth Element and Twenty-One other Trace Element Concentrations in the Natural River Water
684 Reference Material SLRS-5 (NRC-CNRC), *Geostand Geoanal Res*, 37, 449–467,
685 <https://doi.org/10.1111/j.1751-908X.2013.00232.x>, 2013.
- 686 Yeghicheyan, D., Aubert, D., Bouhnik-Le Coz, M., Chmeleff, J., Delpoux, S., Djouaev, I., Granier, G.,
687 Lacan, F., Piro, J.-L., Rousseau, T., Cloquet, C., Marquet, A., Menniti, C., Pradoux, C., Freydier, R.,
688 Vieira da Silva-Filho, E., and Suchorski, K.: A New Interlaboratory Characterisation of Silicon, Rare
689 Earth Elements and Twenty-Two Other Trace Element Concentrations in the Natural River Water
690 Certified Reference Material SLRS-6 (NRC-CNRC), *Geostand Geoanal Res*, 43, 475–496,
691 <https://doi.org/10.1111/ggr.12268>, 2019.
- 692 Zoller, W. H., Gladney, E. S., and Duce, R. A.: Atmospheric Concentrations and Sources of Trace
693 Metals at the South Pole, *Science*, 183, 198–200, <https://doi.org/10.1126/science.183.4121.198>,
694 1974.
- 695